

# Modelling of bacteriophage capsids and free nucleic acids

Peter Zipper<sup>a</sup> and Helmut Durchschlag<sup>b\*</sup>

Received 16 August 2006

Accepted 3 February 2007

<sup>a</sup>Physical Chemistry, Institute of Chemistry, University of Graz, Heinrichstrasse 28, A-8010 Graz, Austria, and<sup>b</sup>Institute of Biophysics and Physical Biochemistry, University of Regensburg, Universitätsstrasse 31, D-93040 Regensburg, Germany. Correspondence e-mail: helmut.durchschlag@biologie.uni-regensburg.de

The reconstruction of sphere shells as realized in bacteriophage capsids can be achieved by *ab initio* modelling approaches based on a genetic algorithm or simulated annealing. The application of tight constraints such as icosahedral symmetry makes the *DAMMIN* procedure the method of choice. The *ab initio* models obtained may be compared with three-dimensional models derived from crystal data. This information, in conjunction with surface calculations and application of specific hydration algorithms, allows the generation of biophysically relevant hydrated three-dimensional models. Modelling free RNA of viruses represents another challenge to advanced modelling intentions. While application of the *DAMMIN* procedure provides the generation of appropriate models for the overall structure of nucleic acids, inclusion of further constraints improves the biological relevance of the resultant models. This may be achieved by our in-house program *SUBSTRUCT*, which allows involvement of secondary structure details.

© 2007 International Union of Crystallography  
Printed in Singapore – all rights reserved

## 1. Introduction

Bacteriophages are viruses that attack bacteria. They consist of a protein coat (the capsid) surrounding the genetic material, which is DNA or RNA, single- or double-stranded. Because of their biological relevance, phages and their constituents have been subject of manifold structural investigations including small-angle scattering (SAS) (Zipper, 1982).

In the context of automated SAS-based modelling of biopolymer structures, the available *ab initio* approaches applying simulated annealing (SA), genetic algorithms (GA) or Monte Carlo simulations have been tested and compared (Zipper & Durchschlag, 2003; Takahashi *et al.*, 2003; Zipper *et al.*, 2005). Since for such tests mainly compact, globular proteins have been used to date, the *ab initio* prediction of structures such as protein shells or free nucleic acids poses a new challenge.

For our studies, empty capsids (artificial top component: ATC) of the *E. coli* phage fr and free RNA of the *E. coli* phage MS2 were used as model systems. The phages fr and MS2 are closely related isometric viruses. Their shape is nearly spherical, featuring icosahedral symmetry; 180 copies of a coat protein of 129 amino-acid (AA) residues form a shell around a single-stranded RNA molecule. The viruses and their components have been subject of intense SAS investigations (*e.g.* Zipper *et al.*, 1971, 1973, 1975; Zipper, 1982; Ribitsch *et al.*, 1985; Kuzmanovic *et al.*, 2003). The crystal structures of bacteriophage MS2 and of fr capsids have been resolved (Golmohammadi *et al.*, 1993; Liljas *et al.*, 1994).

The ATC of the *E. coli* phage fr (Zipper *et al.*, 1973) has a molar mass,  $M$ , of approximately  $2480 \text{ kg mol}^{-1}$ , a radius of gyration,  $R_G$ , of 12.0 nm, and sediments with 42 S; it exhibits radial dimensions practically identical to those of the virus (inner and outer diameter of 21.2 and 26.4 nm, respectively, assuming a homogeneous hollow-sphere model). The atomic coordinates of the fr capsids (Liljas *et al.*,

1994) are stored in entry 1FRS of the Protein Data Bank (Berman *et al.*, 2000).

The high-molecular-weight RNA isolated from the *E. coli* phage MS2 is 3569 nucleotides long (corresponding to  $M$  of about  $1200 \text{ kg mol}^{-1}$ ); it exhibits 73% base pairing due to its ability to fold back on itself and form rigid double-helical segments besides more flexible unpaired regions. Its secondary structure resembles a 'bouquet of flowers' (Fiers *et al.*, 1976). The scattering behaviour of the free RNA mirrors the constituent rod-like segments. The small-angle X-ray scattering (SAXS) curve in the presence of  $\text{Mg}^{2+}$  (Zipper *et al.*, 1975; Zipper, 1982) was interpreted in terms of a rather loose structure, resembling an elongated flat particle of about 62 nm diameter and  $R_G$  of about 18 nm; two cross-section factors, yielding the parameters  $R_{G,c}$  and  $M_c$  due to the overall shape and the specific substructure of the molecule, and one thickness factor were found. The hydrodynamic behaviour was characterized by a sedimentation coefficient of 26.6 S and an intrinsic viscosity  $[\eta]$  of  $44.0 \text{ cm}^3 \text{ g}^{-1}$  (Slegers *et al.*, 1973). Previous model calculations (Zipper *et al.*, 1975) already considered linear segments of different lengths to simulate single-stranded and double-helical segments, and finally led to some kind of coil-like structure allowing a certain amount of flexibility. Recent pilot tests to model free MS2 RNA by *ab initio* approaches were also successful, but pointed out several modelling problems (Zipper *et al.*, 2005).

The present investigations concentrate on modelling ATC and MS2 RNA by efficient *ab initio* approaches, the SA-based program *DAMMIN* (Svergun, 1999, 2000) and the GA-based program *DALAI\_GA* (Chacón *et al.*, 1998, 2000). For advanced conventional modelling of free RNA, the previously used algorithm (Zipper *et al.*, 1975; Zipper, 1982) was improved (program *SUBSTRUCT*). The crystal data for the bacteriophage fr capsids (Liljas *et al.*, 1994) were used to create anhydrous and, by means of special hydration algorithms (Durchschlag & Zipper, 2005), also hydrated three-dimen-

sional models. Finally, hydrodynamic parameters were predicted by using the program *HYDRO* (García de la Torre *et al.*, 1994, 2000; Zipper *et al.*, 2005).

## 2. Modelling approaches and parameter predictions

The underlying *ab initio* modelling approaches have been summarized previously (Svergun & Koch, 2003; Koch *et al.*, 2003; Zipper & Durchschlag, 2003; Zipper *et al.*, 2005). The calculation procedures required for the creation of surface areas and hydrated models are reviewed elsewhere (Durchschlag & Zipper, 2005). In contrast, the in-house program *SUBSTRUCT* represents a novel adaptation of a modelling approach for particles permanently changing their shape. In brief:

The program *DALAI\_GA* (Chacón *et al.*, 1998, 2000) uses an iterative fitting of scattering curves by a GA. It gradually explores a discrete search space and evolves convergent bead models fitting the experimental target curve up to  $h_{\max} = \pi/(2r_b)$ ; the models are refined by gradually reducing the bead radius  $r_b$  and adapting the search space in successive cycles.

The program *DAMMIN* (Svergun, 1999, 2000) starts with a predefined search space (usually a sphere) filled with densely packed dummy atoms (equally sized spheres). SA is used as a global minimization algorithm that finally achieves a particle configuration matching the entire experimental scattering curve entered by a *GNOM* file (Svergun, 1992).

For the alignment and superposition of best-matching *ab initio* models and subsequent averaging, the program package *DAMAVR* (Volkov & Svergun, 2003) was used; in the case of MS2 RNA in-house programs were also applied (Zipper *et al.*, 2005).

The program *SUBSTRUCT* is the improved implementation of a Monte Carlo algorithm developed previously (Zipper *et al.*, 1975) for modelling the scattering behaviour of single-stranded RNAs. In the program, the single-stranded and the double-helical segments are modelled as linear arrangements of beads of equal size but different weight. The modelling procedure is governed by a few adjustable input parameters. The evolution of model configurations within a given search space is completely directed by random numbers and performed in two cycles: initially, all single-stranded segments are created; in the second cycle the positioning of the double-helical segments is fixed. The creation of more complex structures, such as 'L'-shaped molecules, is achieved by combining search rooms differing in nature (*e.g.* sphere, ellipsoid, cylinder), size and mutual position and orientation. The total number of beads ( $N_b$ ) and the partitioning into single- and double-strand segments with appropriate weighting of the beads are chosen in accordance with the underlying SAXS data (*e.g.* mass per unit length,  $M_c$ ).

The experimental SAXS profiles and the models derived therefrom already contain hydration contributions. In contrast, three-dimensional models derived from crystallographic data are anhydrous models; the few water molecules mentioned in the crystallographic databases are usually inadequate for modelling studies (Durchschlag & Zipper, 2003). The combination of surface calculation programs such as *SIMS* (Vorobjev & Hermans, 1997) and special hydration algorithms (in-house programs *HYDCRYST* and *HYDMODEL*; Durchschlag & Zipper, 2001, 2002, 2003) allows the construction of biophysically realistic hydrated three-dimensional models for different hydration levels.

The calculation of SAXS intensities,  $I(h)$ , and pair-distance distribution functions,  $p(r)$ , from the coordinates of the spheres and the computation of structural parameters were performed by means

of Debye's formula and the algorithms described previously (Glatter, 1980; Glatter & Kratky, 1982). Hydrodynamic parameters (sedimentation and translational diffusion coefficients,  $s$  and  $D$ , and intrinsic viscosity,  $[\eta]$ ) were obtained by a modified version of the program *HYDRO* (García de la Torre *et al.*, 1994, 2000; Zipper *et al.*, 2005); models composed of a huge number of spheres additionally required a reduction step. Previous tests have proven the validity of the applied reduction procedures (Zipper *et al.*, 2005; Durchschlag & Zipper, 2005).

The obtained models were visualized by *RASMOL* (Sayle & Milner-White, 1995). Surface representations used programs from the *CCP4* package (Collaborative Computational Project, No. 4, 1994); the electron densities were displayed by *VOLVIS* (Avila *et al.*, 1994).

## 3. Results and discussion

The above-mentioned modelling approaches were applied to the experimentally investigated samples (fr capsid, MS2 RNA) and to various models.

(i) In particular, the following *ab initio* models (*DALAI\_GA* and *DAMMIN*) and three-dimensional reconstructions of the capsid were under analysis: ATC: experimentally studied capsid; model A: sphere-shell model built from 180 spheres; capsid, reduced: anhydrous model of the shell based on 1FRS, reduced to a practicable number of spheres; SU-capsid: anhydrous model of the shell based on 1FRS, reduced to exactly 180 spheres; SC0: hydrated model for the capsid based on 1FRS, low hydration level; SC9: hydrated model for the capsid based on 1FRS, high hydration level. For the calculation of scattering functions and hydrodynamic parameters, SC0 and SC9 had also to be reduced, in particular because of the huge number of water molecules (up to > 40 000) involved. (ii) In the case of MS2 RNA, the investigations comprise: the experimentally studied RNA; *DALAI\_GA* models; *DAMMIN* models; *SUBSTRUCT* models.

### 3.1. Modelling the empty capsid by *ab initio* approaches

All *ab initio* approaches tested were able to reconstruct the hollow-sphere nature of the capsid, however, with different success (Fig. 1). Application of *DALAI\_GA* in context with a spherical search space (S) yielded a rather incomplete hollow-sphere structure (not shown),

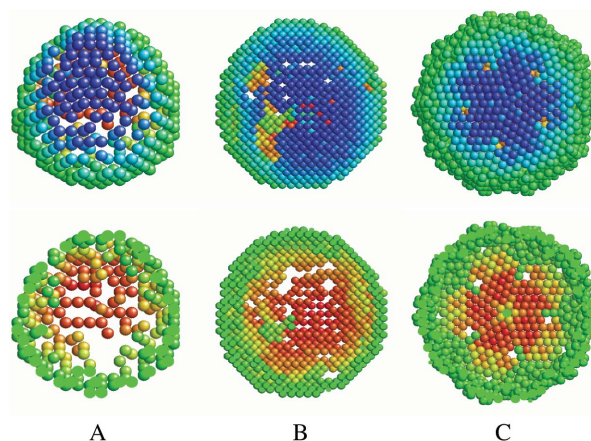


**Figure 1**  
Selected reconstructions of ATC, generated by *DALAI\_GA* (A) or by *DAMMIN* (B, C). The lower row shows central slabs of the models in the upper row. Different colourings reflect the assembling of the models along the  $z$  axis. Calculation details: A: *DALAI\_GA*, hollow sphere as search space,  $N_b = 495$ ,  $r_b = 0.95$  nm; B: *DAMMIN*, spherical search space, P1U (no symmetry constraint),  $N_b = 1961$ ,  $r_b = 0.65$  nm; C: *DAMMIN*, spherical search space, PicoU (icosahedral symmetry),  $N_b = 2043$ ,  $r_b = 0.65$  nm.

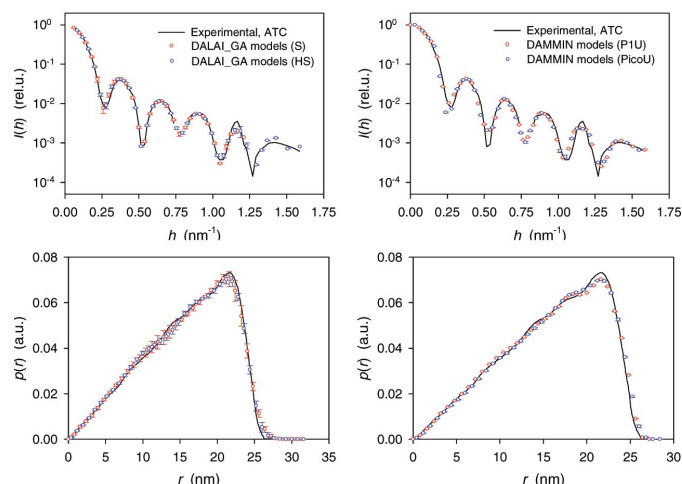


**Figure 2**  
Comparison of experimental SAXS profiles of ATC and the averaged profiles of *DALAI\_GA* (left) and *DAMMIN* (right) reconstructions.

while use of a hollow-sphere search space (HS) forced the creation of a hollow-sphere model exhibiting only slight deficiencies (some holes as shown in Fig. 1A). In contrast, application of *DAMMIN* resulted in the reconstruction of more appropriate capsid models (Fig. 1B, C). While usage of icosahedral constraints (PicoU) yielded a perfect reconstruction (Fig. 1C), even application of unconstrained modelling (P1U) gave reasonable models (Fig. 1B). With both approaches, the fit of the  $I(h)$  and  $p(r)$  patterns came up to expectations (Fig. 2).

The reconstruction of specially constructed models yielded similar results. Again, the *DAMMIN* models were superior to the *DALAI\_GA* models (Fig. 3). As with the experiment-based models, the comparison of the SAXS profiles of the models was satisfying with both *ab initio* approaches (Fig. 4).

### 3.2. Anhydrous and hydrated three-dimensional models of capsids

The creation of anhydrous models based on the available crystallographic data (Fig. 5A) revealed that the above *ab initio* SAXS models, indeed, show a striking resemblance to the three-dimensional models. Hydrated models (Figs. 5B and C) bespeak the localization of possible water sites on the protein inner and outer surface. Irre-

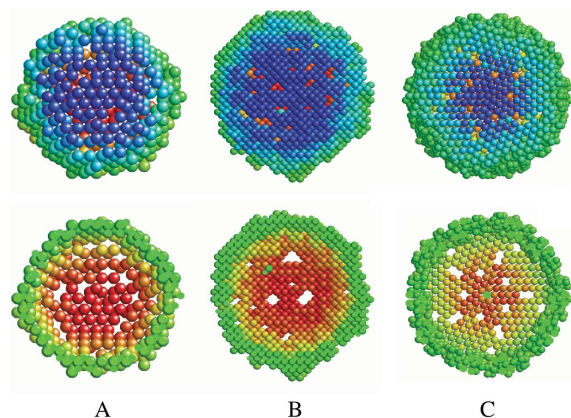


**Figure 3**  
Selected reconstructions of model A, generated by *DALAI\_GA* (A) or by *DAMMIN* (B, C). The lower row shows central slabs of the models in the upper row. Different colourings reflect the assembling of the models along the  $z$  axis. Calculation details: A: *DALAI\_GA*, hollow sphere as search space,  $N_b = 580$ ,  $r_b = 1.0$  nm; B: *DAMMIN*, spherical search space, P1U,  $N_b = 2336$ ,  $r_b = 0.65$  nm; C: *DAMMIN*, spherical search space, PicoU,  $N_b = 1965$ ,  $r_b = 0.65$  nm.

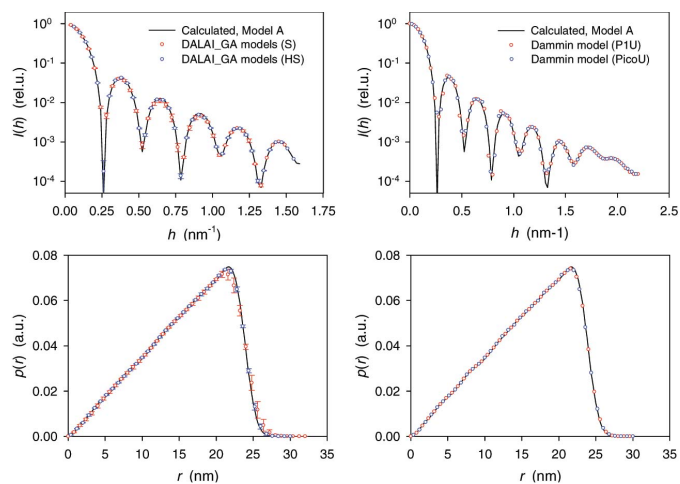


**Figure 4**  
Comparison of the SAXS profiles of model A and the (averaged) profiles of *DALAI\_GA* (left) and *DAMMIN* (right) reconstructions.

spective of the level of hydration, the protein envelope is not completely covered by water molecules. Moreover, the fine structure of the hydrated models hints at some channels in the protein coat.

The comparison of the SAXS profiles of various analysed models (Fig. 6) shows good agreement with the experimental curves, except the SU-capsid model which obviously suffers in this case from the enormous reduction performed in a single step. As expected, the influence of water molecules on the scattering behaviour is only marginal, owing to their small size in comparison to the large capsids (Durchschlag & Zipper, 2003, 2005).

### 3.3. Modelling the free nucleic acid by *ab initio* approaches

Applying the *ab initio* approaches *DALAI\_GA* and *DAMMIN* to RNA in a manner similar to that adopted for proteins yielded more or less realistic models for the overall shape of the nucleic acid (Zipper *et al.*, 2005). A few representative images are depicted in Fig. 7. The *ab initio* approaches clearly establish the bent structure of RNA and an uneven surface, similar to the *DAMMIN* models found for rRNA (Funari *et al.*, 2000); details of surface characteristics get lost. Essentially the same features are obtained by applying surface

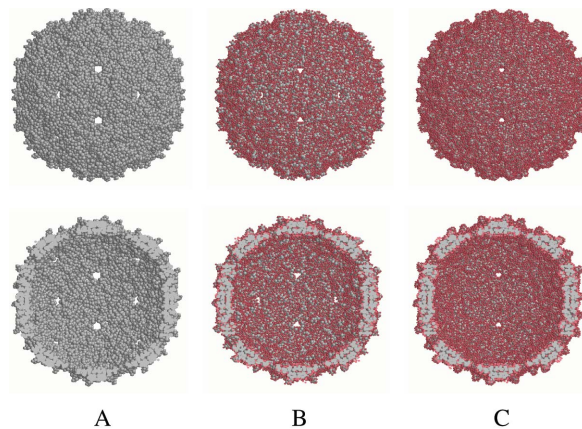


**Figure 5**  
Anhydrous and hydrated three-dimensional models of capsids, together with their central slabs. The 23 220 AA residues (grey) of the anhydrous model (A) were constructed on the basis of 1FRS. The hydrated models, created by use of *SIMS* and *HYDROMODEL*, show additionally the water molecules (pink) for low (B) and high (C) hydration levels (models SC0 and SC9).

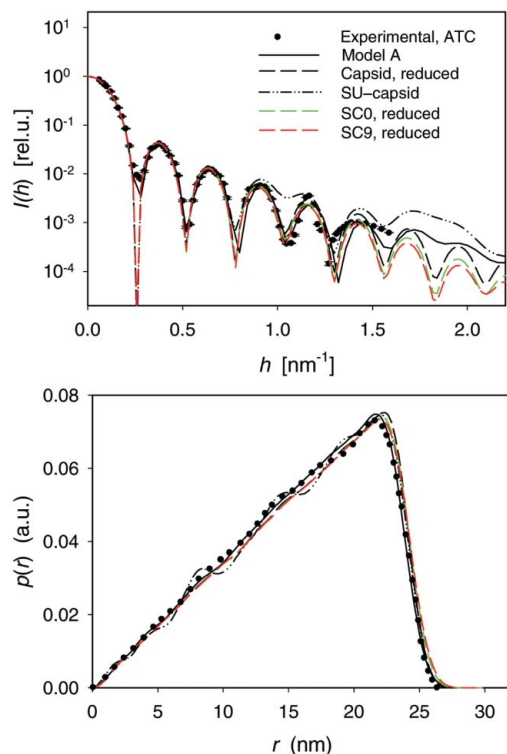


**Figure 6**  
Comparison of scattering profiles of anhydrous and hydrated capsid models.

rendering techniques as those inherent in the *CCP4* package. The agreement of observed and predicted scattering profiles has already been described (Zipper *et al.*, 2005).

### 3.4. Modelling the free nucleic acid by *SUBSTRUCT*

Modelling the shape of free RNA by *SUBSTRUCT* allows the reconstruction of biophysically possible models. Probing the applicability of various modelling strategies of *SUBSTRUCT* (Fig. 8) allowed the realization of models with a secondary structure consisting of certain amounts of single- and double-stranded regions and including L-shaped structures and loops. To take account of the flexibility of the RNA molecules, the scattering functions of selected models have to be averaged. Only the averages of  $I(h)$  and  $p(r)$  (Fig. 9), not the functions of individual models, are considered to be of relevance and are used to fit the experimental functions as far as possible. The decisive criterion for selecting a model under consideration is its ability to improve the global fit to the target curves. Best models were obtained after inclusion of the mentioned special molecular characteristics.

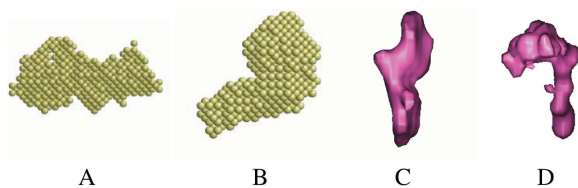


**Figure 7**  
Averaged models for MS2 RNA obtained by *DALAI\_GA* (A) or *DAMMIN* (B) and surface representations of averaged models created by *DALAI\_GA* (C) and *DAMMIN* (D). For calculation details *cf.* Zipper *et al.* (2005).

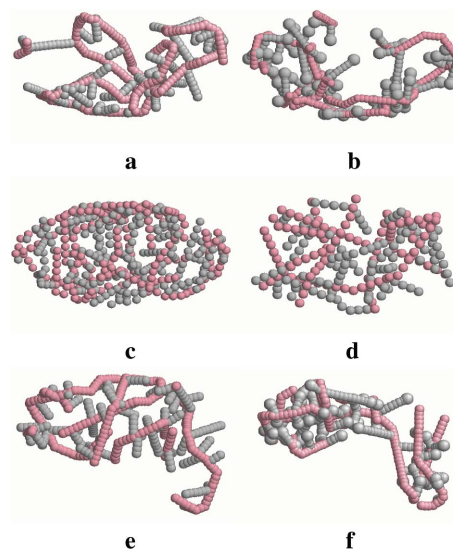


**Figure 8**  
Selected *SUBSTRUCT* models of MS2 RNA, obtained by applying different modelling strategies: variation of the search space (a–d: single elliptic cylinders, e, f: combinations of two elliptic cylinders); variation of the radius, next-neighbour distance ( $\Delta$ ), and total number of beads [a–f:  $r_b = 1.3$  nm, except for the enlarged terminal beads ('hairpin loops') of the double-stranded branches in models b and f, where  $r_b = 1.83$  nm; a, b and e, f:  $\Delta = 1.3$  nm, c, d:  $\Delta = 2.6$  nm; a–c and e, f:  $N_b = 456$ , d:  $N_b = 248$ ]; variation of the simulated double-helix content (a: 72.3%; b–f: 74.7%). Single-stranded RNA (weighting factor 1.0) is coloured in pink and double-stranded branches (weighting factor 2.77) are shown in grey.

### 3.5. Prediction of structural and hydrodynamic parameters

Besides the visual inspection of the obtained models and fitted SAXS profiles, the validity of the resultant model bodies has to be checked by quantifying the results in terms of structural and hydrodynamic parameters (such as  $V$ ,  $R_G$ ,  $d_{max}$ ,  $s$ ,  $D$  and  $[\eta]$ ). As may be taken from Table 1, the parameter predictions turn out to be quite satisfactory. A closer look at the data, again, reveals the high quality of the *DAMMIN* approach, and in the case of free RNA also of *SUBSTRUCT*. It bespeaks, however, also a distinct overestimation of  $s$  and an underestimation of  $[\eta]$  in comparison with the experimentally found data in the case of MS2 RNA, and a less pronounced overestimation of  $s$  for ATC. The observed discrepancies between the experimental value for  $d_{max}$  of ATC and the tabulated  $d_{max}$  values of ATC, model A and the models derived from the crystal structure are mainly due to the fact that the experimental value was based on the idealized assumption of a homogeneous spherical shell (Zipper *et al.*, 1973), whereas the  $d_{max}$  values in Table 1 represent the maximum vertex-to-vertex distances in bead models.

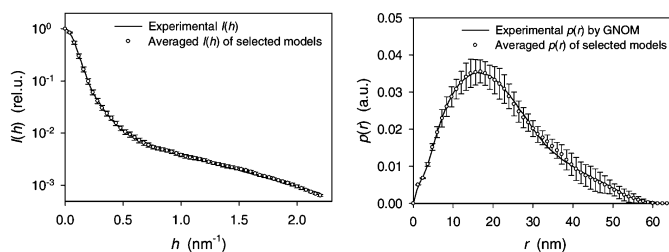


**Figure 9**  
Comparison of the experimental scattering profiles of MS2 RNA with the averaged profiles of 12 *SUBSTRUCT* models exhibiting hairpin loops and the other features presented in Fig. 8a,b.

**Table 1**  
Comparison of calculated structural and hydrodynamic parameters.

	$N_b$	$r_b$ (nm)	$V$ (nm <sup>3</sup> )	$R_G$ (nm)	$d_{max}$ (nm)	$D$ (10 <sup>-7</sup> cm <sup>2</sup> s <sup>-1</sup> )	$s$ (10 <sup>-13</sup> s)	$[\eta]$ (cm <sup>3</sup> g <sup>-1</sup> )
ATC								
<i>DALAI_GA</i> (S)†	66–279	2.2–1.25‡	3700 (700)	12.0 (1)	30.6 (8)	1.64 (2)	44.3 (5)	5.6 (2)
<i>DALAI_GA</i> (HS)†	171–495	1.5–0.95‡	3100 (400)	11.99 (9)	29.8 (12)	1.65 (2)	44.6 (5)	5.5 (2)
<i>DAMMIN</i> (P1U)	1968 (10)	0.65‡	3060 (20)	12.02 (0)	27.9 (0)	1.649 (0)	44.5 (0)	5.68 (0)
<i>DAMMIN</i> (PicoU)	1953 (153)	0.65‡	3030 (240)	12.12 (2)	28.5 (2)	1.617 (8)	43.6 (2)	6.02 (9)
Model A								
<i>DALAI_GA</i> (S)†	70–496	2.15–1.05‡	4100 (800)	12.12 (6)	30.8 (10)	1.62 (3)	43.6 (7)	5.9 (3)
<i>DALAI_GA</i> (HS)†	204–580	1.5–1.0‡	3500 (200)	12.06 (2)	29.8 (6)	1.64 (1)	44.2 (3)	5.7 (1)
<i>DAMMIN</i> (P1U)	2336	0.65‡	3630	12.04	29.8	1.629	44.0	5.94
<i>DAMMIN</i> (PicoU)	1965	0.65‡	3050	12.03	30.0	1.614	43.6	6.03
Capsid, reduced§	5820	0.24–0.69	3000	12.18	28.95	1.656	44.6	6.02
SC0, reduced§	7827	0.18–0.70	3770	12.21	29.64	1.664	44.8	6.28
SC9, reduced§	8253	0.18–0.70	4040	12.22	29.64	1.661	44.7	6.41
SU-capsid	180	1.58	3000	12.12	27.69	1.699	45.7	5.16
MS2 RNA								
<i>DALAI_GA</i> (ellipsoid)†¶	89–200	2.0–1.25‡	3100 (700)	16.7 (4)	63.1 (27)	1.31 (2)	31.9 (5)	30.4 (18)††
<i>DAMMIN</i> (P1U/O/P)‡‡	187 (4)	1.5‡	3580 (70)	17.2 (3)	59.7 (17)	1.26 (3)	30.6 (7)	34.3 (22)††
<i>SUBSTRUCT</i> §§	456	1.3 [1.83]¶¶	3260	17.4 (12)	61.2 (23)	1.29 (3)	31.4 (7)	32.3 (19)††

† The averages include all pertinent *DALAI\_GA* models obtained, irrespective of the size and number of beads; the limiting values for  $N_b$  and the bead radii  $r_b$  are given. ‡ For the calculation of parameters, the nominal values of  $r_b$  were increased by a factor of 1.105 to account for the packing density of the beads. § The model consists of beads differing in size; the limiting values for  $r_b$  are given. ¶ The search space was of oblate ellipsoidal shape. †† This value was obtained after applying a volume correction. ‡‡ The averages include all *DAMMIN* models obtained, irrespective of the shape bias (unknown, oblate, prolate). §§ The averages include selected models with hairpin loops simulated by an enlarged bead terminating the double strands. ¶¶ The value given in brackets refers to the terminal bead in double strands; to optimize the fit of the averaged scattering profiles, the nominal bead radii were decreased by a factor of 0.86 and the coordinates by a factor of 0.98.

#### 4. Conclusions

The *ab initio* approaches applied to ATC and free MS2 RNA obviously allow the reconstruction of realistic particle shapes: hollow-sphere models for the phage envelopes and coil-like entities for free RNA that is, however, composed of differently compact regions. *Ab initio* models for ATC could be improved by applying hollow-sphere or icosahedral constraints. Results for ATC were compared with three-dimensional models from the crystal data of the capsid, and those for MS2 RNA to additional surface renderings and *SUBSTRUCT* models. The results found for MS2 RNA confirm a loose RNA structure, allowing some flexibility of the free RNA molecule (uneven surface, bent structure composed of single- and double-stranded regions). The models obtained by *SUBSTRUCT* could be sharpened by special selection criteria for the averaging procedures to be applied. As a quantitative criterion for the accuracy of the models obtained, a comparison of a variety of structural and hydrodynamic parameters was executed, in addition to a comparative inspection of the  $I(h)$  and  $p(r)$  functions. Applying appropriate selection and averaging criteria, fair agreement between experimental and predicted parameters was achieved, and an equally well conformity between the models could be established.

The authors are much obliged to several scientists for use of their computer programs: to P. Chacón for *DALAI\_GA*, to D. I. Svergun for *DAMMIN*, the *DAMMAVER* suite and *GNOM*, to Y. N. Vorobjev for *SIMS*, to J. García de la Torre for *HYDRO*, to R. A. Sayle for *RASMOL*, to the SERC Daresbury Laboratory for the *CCP4* suite, and to the Research Foundation of the State University of New York for *VOLVIS*, respectively.

#### References

Avila, R., He, T., Hong, L., Kaufman, A., Pfister, H., Silva, C., Sobierajski, L. & Wang, S. (1994). *Proceedings IEEE Visualization '94*, edited by R. Bergeron & A. Kaufman, pp. 31–38. Washington DC: IEEE Computer Society.  
 Bertram, H. M., Westbrook, J., Feng, Z., Gilliland, G., Bhat, T. N., Weissig, H., Shindyalov, I. N. & Bourne, P. E. (2000). *Nucleic Acids Res.* **28**, 235–242.  
 Chacón, P., Díaz, J. F., Morán, F. & Andreu, J. M. (2000). *J. Mol. Biol.* **299**, 1289–1302.

Chacón, P., Morán, F., Díaz, J. F., Pantos, E. & Andreu, J. M. (1998). *Biophys. J.* **74**, 2760–2775.  
 Collaborative Computational Project, Number 4 (1994). *Acta Cryst. D* **50**, 760–763.  
 Durchschlag, H. & Zipper, P. (2001). *Biophys. Chem.* **93**, 141–157.  
 Durchschlag, H. & Zipper, P. (2002). *J. Phys. Condens. Matter*, **14**, 2439–2452.  
 Durchschlag, H. & Zipper, P. (2003). *Eur. Biophys. J.* **32**, 487–502.  
 Durchschlag, H. & Zipper, P. (2005). *Analytical Ultracentrifugation: Techniques and Methods*, edited by D. J. Scott, S. E. Harding & A. J. Rowe, pp. 389–431. Cambridge: Royal Society of Chemistry.  
 Fiers, W., Contreras, R., Duerinck, F., Haegeman, G., Iserentant, D., Merregaert, J., Min Jou, W., Molemans, F., Raeymaekers, A., Van den Berghe, A., Volckaert, G. & Ysebaert, M. (1976). *Nature (London)*, **260**, 500–507.  
 Funari, S. S., Rapp, G., Perbandt, M., Dierks, K., Vallazza, M., Betzel, C., Erdmann, V. A. & Svergun, D. I. (2000). *J. Biol. Chem.* **275**, 31283–31288.  
 García de la Torre, J., Huertas, M. L. & Carrasco, B. (2000). *Biophys. J.* **78**, 719–730.  
 García de la Torre, J., Navarro, S., López Martínez, M. C., Díaz, F. G. & López Cascales, J. J. (1994). *Biophys. J.* **67**, 530–531.  
 Glatter, O. (1980). *Acta Phys. Austriaca*, **52**, 243–256.  
 Glatter, O. & Kratky, O. (1982). Editors. *Small Angle X-ray Scattering*. London: Academic Press.  
 Golmohammadi, R., Valegård, K., Fridborg, K. & Liljas, L. (1993). *J. Mol. Biol.* **234**, 620–639.  
 Koch, M. H. J., Vachette, P. & Svergun, D. I. (2003). *Q. Rev. Biophys.* **36**, 147–227.  
 Kuzmanovic, D. A., Elashvili, I., Wick, C., O'Connell, C. & Krueger, S. (2003). *Structure*, **11**, 1339–1348.  
 Liljas, L., Fridborg, K., Valegård, K., Bundule, M. & Pumpens, P. (1994). *J. Mol. Biol.* **244**, 279–290.  
 Ribitsch, G., De Clercq, R., Folkhard, W., Zipper, P., Schurz, J. & Clauwaert, J. (1985). *Z. Naturforsch.* **40c**, 234–241.  
 Sayle, R. A. & Milner-White, E. J. (1995). *Trends Biochem. Sci.* **20**, 374–376.  
 Slegers, H., Clauwaert, J. & Fiers, W. (1973). *Biopolymers*, **12**, 2033–2044.  
 Svergun, D. I. (1992). *J. Appl. Cryst.* **25**, 495–503.  
 Svergun, D. I. (1999). *Biophys. J.* **76**, 2879–2886.  
 Svergun, D. I. (2000). *J. Appl. Cryst.* **33**, 530–534.  
 Svergun, D. I. & Koch, M. H. J. (2003). *Rep. Prog. Phys.* **66**, 1735–1782.  
 Takahashi, Y., Nishikawa, Y. & Fujisawa, T. (2003). *J. Appl. Cryst.* **36**, 549–552.  
 Volkov, V. V. & Svergun, D. I. (2003). *J. Appl. Cryst.* **36**, 860–864.  
 Vorobjev, Y. N. & Hermans, J. (1997). *Biophys. J.* **73**, 722–732.  
 Zipper, P. (1982). *Small Angle X-ray Scattering*, edited by O. Glatter & O. Kratky, pp. 295–328. London: Academic Press.  
 Zipper, P. & Durchschlag, H. (2003). *J. Appl. Cryst.* **36**, 509–514.

## conference papers

---

Zipper, P., Durchschlag, H. & Krebs, A. (2005). *Analytical Ultracentrifugation: Techniques and Methods*, edited by D. J. Scott, S. E. Harding & A. J. Rowe, pp. 320–371. Cambridge: Royal Society of Chemistry.

Zipper, P., Folkhard, W. & Clauwaert, J. (1975). *FEBS Lett.* **56**, 283–287.

Zipper, P., Kratky, O., Herrmann, R. & Hohn, T. (1971). *Eur. J. Biochem.* **18**, 1–9.

Zipper, P., Schubert, D. & Vogt, J. (1973). *Eur. J. Biochem.* **36**, 301–310.